Measurement of Flow Characteristics in a Bubbling Fluidized Bed Using Electrostatic Sensor Arrays

Wenbiao Zhang, *Member, IEEE*, Yong Yan, *Fellow, IEEE*, Yongrong Yang, and Jingdai Wang

***Abstract*— Fluidized beds are widely applied in a range of industrial processes. In order to maintain the efficient operation of a fluidized bed, the flow parameters in the bed should be monitored continuously. In this paper, electrostatic sensor arrays are used to measure the flow characteristics in a bubbling fluidized bed. In order to investigate the electrostatic charge distribution and the flow dynamics of solid particles in the dense region, time and frequency domain analysis of the electrostatic signals is conducted. In addition, the correlation velocities and weighted average velocity of Geldart A particles in the dense and transit regions are calculated, and the flow dynamics of Geldart A and D particles in the dense and transit regions are compared. Finally, the influence of liquid antistatic agents on the performance of the electrostatic sensor array is investigated. According to the experimental results, it is proved that the flow characteristics in the dense and transit regions of a bubbling fluidized bed can be measured using electrostatic sensor arrays.**

***Index Terms*— Bubbling fluidized bed, electrostatic sensor, liquid antistatic agent (LAA), solids velocity, time and frequency domain analysis.**

I. Introduction

FLUIDIZED beds, which have excellent heat and mass transfer rate and the ability of handling a high volume of particles, have been widely applied in the chemical, pharmaceutical, and energy industries. In order to maintain the efficient operation of the process, flow dynamics of the particles in the bed should be monitored. The velocity and concentration of solid particles are two important parameters of the flow dynamics in the fluidized bed, which influence the residence time, mixing, heat and mass transfer, and erosion in the bed. Several techniques have been used for the measurements of the velocity and concentration of solid particles in the bed. Van Ommen and Mudde [1] reviewed and appraised the techniques, such as direct visualization, tomography, optical probes, capacitance probes, and pressure measurements, to determine the gas–solid distribution in fluidized beds. Besides, as a nonintrusive method, acoustic emission has also been applied to the monitoring of fluidized beds [2]–[4]. Based on the energy distribution and power spectra of the acoustic signals, the particle motion, flow pattern, and stability of the bed were monitored.

Electrostatic charge is generated due to the interactions between particles and the frictions between particles and walls of the bed. The excess accumulation of electrostatic charge can influence the hydrodynamics of the fluidized bed significantly, including the generation of particle agglomerations and wall sheeting [5]. However, the electrostatic phenomena can be used to develop sensors for the measurements of the flow parameters of a fluidized bed. Based on the principle of electrostatic induction, electrostatic sensors have been widely applied to the measurement of solid flow in the pneumatic conveying pipelines [6]–[12]. The velocity, concentration, and mass flow rate of particles can be measured using ring, arc, and intrusive electrodes. Although the application of electrostatic sensors to the measurement of solid particles in a pneumatic conveying pipeline is successful, solids flow behaviors in a fluidized bed are still not fully understood due to their inherent complexity. Therefore, investigations should be conducted to evaluate the performance of electrostatic sensors for the measurement of solid particles in a fluidized bed. Some attempts have already been made in this area [13]–[16]. Portoghese *et al.* [13] used an intrusive electrostatic probe to measure the moisture content in a fluidized bed-based drying process. The relationship between the electrostatic signal and moisture content was established, which was sensitive to the moisture content of 100 ppm. Zhang *et al.* [14] combined the electrostatic sensor with electrical capacitance tomography to measure the flow dynamics in a triple-bed combined circulating fluidized bed. The flow behaviors in different flow regimes were investigated. He *et al.* [15], [16] developed a dual-tip electrostatic probe for the measurements of particle charge density and bubble properties in bubbling fluidized beds. The estimated particle charge density and bubble rise velocity were in reasonable agreement with those obtained using a Faraday cup and video imaging. However, the intrusive probe may influence the flow behavior in the bed, and the performance of electrostatic sensor on the measurement of flow dynamics in the dense bubbling bed should be investigated.

Particle size distribution and density difference between the gas and solid phases have a significant impact on the fluidization process. Based on a large volume of experimental data,

Manuscript received August 30, 2015; revised November 2, 2015; accepted December 13, 2015. Date of publication January 22, 2016; date of current version February 5, 2016. This work was supported in part by the National Natural Science Foundation of China under Grant 61403138, Grant 21236007, and Grant 21525627, in part by the Chinese Ministry of Science and Technology under Grant 2012CB215203, in part by the Chinese Ministry of Education under Grant B13009, and in part by the Fundamental Research Funds for Central Universities, North China Electric Power University, China, under Grant 2014QN13. The Associate Editor coordinating the review process was Dr. Salvatore Baglio. *(Corresponding author: Yong Yan.)*

W. Zhang is with the School of Control and Computer Engineering, North China Electric Power University, Beijing 102206, China (e-mail: wbzhang@ncepu.edu.cn).

Y. Yan is with the School of Engineering and Digital Arts, University of Kent, Canterbury CT2 7NT, U.K. (e-mail: y.yan@kent.ac.uk).

Y. Yang and J. Wang are with the School of Chemical and Biological Engineering, Zhejiang University, Hangzhou 310027, China (e-mail: yangyr@zju.edu.cn; wangjd@zju.edu.cn).

Color versions of one or more of the figures in this paper are available online at http://ieeexplore.ieee.org.

Digital Object Identifier 10.1109/TIM.2016.2514698

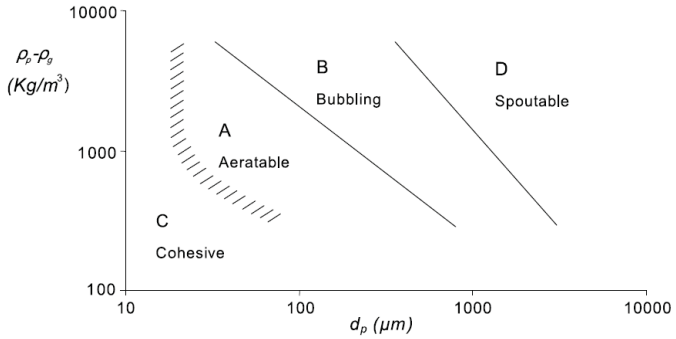

Fig. 1. Geldart diagram adopted from [17].

Geldart [17] classified particles into four types, i.e., Geldart A, B, C, and D particles. The size and density of each type of particles are illustrated in Fig. 1. It is well known that different types of particles have different fluidization characteristics in the bed.

Preliminary results were reported of the measurement of flow parameters in a bubbling fluidized bed for Geldart D particles using electrostatic sensor arrays at the IEEE International Instrumentation Measurement Technology Conference [18]. This paper gives more detailed experimental results along with interpretations. Compared with previous work, it is the first attempt to measure the flow dynamics in the dense-phase gas–solid fluidized bed using electrostatic sensor arrays. In the bubbling fluidized bed, there are three regions, i.e., dense region, transit region, and freeboard. In the dense region, the solid concentration is high and solid particles move mainly upward. The solids in the freeboard are fine particles, which are entrained by the fluidization air. The transit region is in-between the dense region and freeboard, and some of the particles in this region may fall down due to gravity. The electrostatic sensor arrays used in this paper have two groups of electrodes, which are fitted in the dense and transit regions of the bed, respectively. As the electrostatic signals contain much information about the flow dynamics of solid particles in the bed, time and frequency domain analysis of the electrostatic signals is conducted, from which the electrostatic charge distribution and flow behavior in the bed can be characterized. Since the flow behavior in the transit region is very complex, only the signals from dense region are investigated. Besides, cross correlation analysis of the electrostatic signals from different electrodes is performed. The correlation velocities and weighted average velocity of Geldart A particles in the dense and transit regions are calculated. The flow dynamics of Geldart A and D particles in the dense and transit regions are compared.

The electrification of solid particles in a fluidized bed can have a negative impact on the effective operation of the process. However, since electrification of solid particles depends on many factors including particle properties, bed design, and operational and environmental conditions, it is thus difficult to control the electrification of solid particles in the bed. Several attempts have been made in this area. Park *et al.* [19] investigated the reduction of electrostatic charge by increasing the humidity of fluidization air. It was found that the relative humidity between 40% and 80% is the best range for charge elimination. Wang *et al.* [20] found the charge magnitude, and polarity of particles could be changed by adding a small amount of metal oxides into the fluidized bed. Dong *et al.* [21] investigated the electrostatic charge control by injecting a trace of liquid antistatic agents (LAA) into a bubbling fluidized bed and analyzed the electrostatic effect on the hydrodynamics of the bed. All the above methods could regulate the electrification of solid particles in the bed. However, whether such methods will affect the operation of electrostatic sensor arrays is to be investigated.

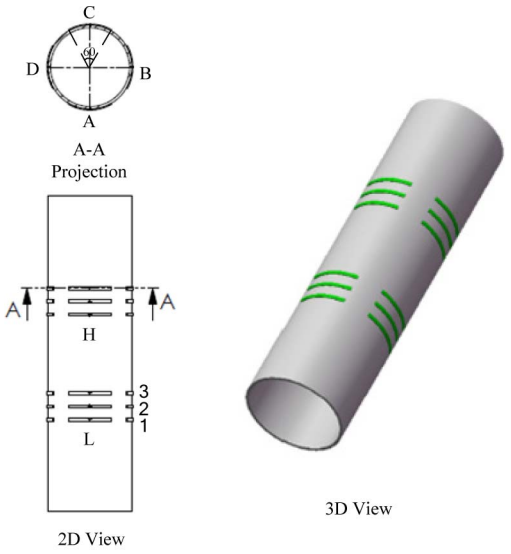

Fig. 2. Design and distribution of the electrostatic sensor arrays.

II. Principle of Measurement

A. Sensor Design and Installation

As a nonintrusive method, the electrostatic senor arrays are installed on the bed wall, which will not disturb the flow behavior in the bed. The sensors are strategically mounted on the bed to measure the flow characteristics in the dense and transit regions of the bed. The physical locations of the sensors in the bed, the distance between adjacent electrodes, and the width and thickness of the electrodes are the key points that must be considered in the design of the sensors. Other factors that should be considered during the design stage include the basic sensing principle of the electrostatic sensor (spatial sensitivity distribution and spatial filtering effect), the requirement of correlation computation, and the flow dynamics of solid particles in the bed. As shown in Fig. 2, the electrostatic sensor arrays used in this paper comprise two groups of electrodes, and each group has four sets and each set has three identical electrodes. One group of electrodes is installed in the dense region of the bubbling fluidized bed while the other group is in the transition region. They are labeled as L group and H group in Fig. 2. The center-to-center distance between the two groups of electrodes is 200 mm. The electrostatic signals from the electrodes are correlated to determine the particle velocities, so the distance between the

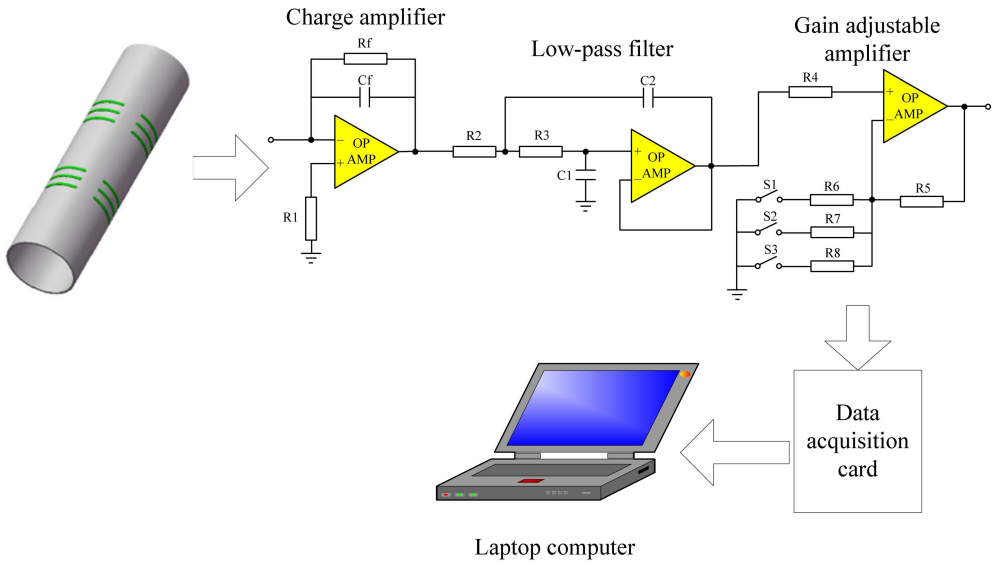

Fig. 3. Schematic of the signal conditioning and processing system.

adjacent electrodes should be reasonably small to maintain good similarity between the two signals [22]. Meanwhile, the spacing between the adjacent electrodes should not be too small to avoid overlapping of the sensing volumes of the two adjacent electrodes. In this design, the distance between the two adjacent electrodes is set to 25 mm. The cross section of the sensor layout is given in Fig. 2. There are four sets of electrodes in the cross section, which are labeled as A, B, C, and D, respectively. According to the spatial filtering effect, the width of the electrode will affect the frequency bandwidth of the electrostatic signal [22], [23]. The wider the electrode, the narrower the bandwidth of the signal. In consideration of the amplitude and bandwidth of the signal, the width and the thickness of each electrode are set to 6 and 2 mm, respectively. The central angle of the electrode is 60°. The electrodes are made of copper and tightly wrapped around the outer surface of the bed. The material of the bed is made of Plexiglas with a thickness of 5 mm and relative permittivity of 2.3. The permittivity of the material and the thickness of the wall will affect the capacitance between the charged particles and the electrode, which will further affect the induced charge on the electrode. Through analysis of the sensitivity distribution of the electrode, it is found that the electrode is more sensitive to the charged particles closer to the electrode, which can provide the localized flow information in the bed [14]. The flow behaviors in different regions of the bed may be characterized by combing the information from all the electrodes in each sensor array.

B. Signal Conditioning and Processing

The electrostatic signals from the sensor arrays are transformed, filtered, and amplified using a signal conditioning and processing system, the schematic of which is shown in Fig. 3. The design of the circuit plays an important part in the performance of the measurement system. The circuit used in this paper has three parts: 1) charge amplifier; 2) low-pass filter; and 3) gain adjustable amplifier. With the fluctuation of electrostatic charges on the particles and the movement of the particles, a minute change in electric current is detected on the electrode. The current is in the range from 30 to 120 nA under the experimental conditions. The current signal is transformed into a voltage signal through an amplifier circuit. The *I/V* gain of the amplifier is $2 \times 10^7\ \Omega^{-1}$. The input resistance of the amplifier is $10^{13}\ \Omega$. The maximum bias current and offset voltage are 0.1 nA and 2 mV, respectively. The voltage signal is then fed into a second-order low-pass filter with a bandwidth of 1000 Hz. Finally, the signal is further amplified through an amplifier with selectable gains of 1.97, 3.47, and 9.82. Under the experimental conditions in this paper, the gain of 1.97 is used. In order to maintain high signal-to-noise ratio, the circuit boards are installed on the electrodes of the sensor arrays using short copper cylinders. All amplified signals from the circuit boards are sampled simultaneously. A grounded metal box is installed outside the insulated electrodes and circuit boards in order to enhance the signal-to-noise ratio.

The electrostatic signal contains rich information about the flow dynamics of the solid phase in the gas–solid flow. Yan *et al.* [7] used the features in the time and frequency domains in conjunction with a neural network to measure the mass flow rate of solid particles in a pneumatic pipeline. Similar features in both time and frequency domains are used to interpret the electrostatic signals from different electrodes in this paper. In the time domain, the root mean square (rms) value of the electrostatic signal is calculated. The electrostatic signal is generated due to the fluctuation of induced charge on the electrode, which is related to the charge on the particles in the sensitivity volume of the electrode. As a result, rms values of the signals from different electrodes are a good indication of the electrostatic charge distribution in different regions of the bed.

The signal from an electrostatic sensor is random in general, so its power spectrum spreads over a range of frequencies. In order to characterize the fluctuation of the power spectrum,

the average frequency of the signal is defined as follows [7]:

$$F = \frac{\sum_{j=1}^{J} p_j f_j}{\sum_{j=1}^{J} p_j} \tag{1}$$

where f_j is the jth discrete frequency of the signal, p_j is the power density of the jth frequency component, and J is the total number of the discrete frequencies in the power spectrum. To characterize the power spectral density (PSD) distribution of the electrostatic signal, both entropy and shape factor of PSD are used. The probability density function of the power spectrum is defined as [7]

$$d_j = \frac{p_j}{\sum_{j=1}^{J} p_j}, \quad (j = 1, 2, \ldots, J). \tag{2}$$

Then the entropy is given by [7]

$$E = -\sum_{j=1}^{J} d_j \log d_j \tag{3}$$

which provides a measure of the distribution pattern of the PSD. The shape factor of the PSD is defined as [7]

$$\mathrm{SF} = \frac{1}{\bar{p}} \sqrt{\frac{1}{J-1} \sum_{j=1}^{J} (p_j - \bar{p})^2} \tag{4}$$

where $\bar{p}$ is the mean of PSD.

The electrostatic sensors combined with correlation signal processing algorithms have been widely applied to the velocity measurement of solid particles [6]. By calculating the transit time between the upstream and downstream signals, the solid velocity can be determined. However, the solids flow in the bubbling fluidized bed is very complex. The flow parameters significantly fluctuate in the bed. As a result, multiple-electrode sensor arrays are adopted to obtain reliable results by fusing the measurements from all the electrodes. Three correlation velocities v_{12}, v_{23}, and v_{13} are then calculated using the signals from the three electrodes in each set of electrostatic sensor arrays. The peaks in the correlation functions, referred to as correlation coefficients r_{12}, r_{23}, and r_{13}, are also determined. The weighted average velocity is obtained by weighting the correlation velocities with their correlation coefficients [6], [8], [11], [22]

$$v_c = \frac{r_{12} \times v_{12} + r_{23} \times v_{23} + r_{13} \times v_{13}}{r_{12} + r_{23} + r_{13}}. \tag{5}$$

However, it is known that the correlation results from an ill-posed correlation function are not acceptable [12]. Nieuwland *et al.* [24] proposed that the correlation velocity should be discarded if the correlation coefficient was less than 0.6. However, there is no standard rule to set the threshold for correlation coefficient. It will depend on the actual industrial process being monitored and the signal-to-noise ratio. In the present research, we found it is appropriate to set the threshold to 0.3, after extensive observations and analysis. In the bubbling fluidized bed, the particle behaviors are very complex, and hence, the resulting correlation velocities fluctuate significantly. In this paper, a correlation velocity is discarded if it deviates from the mean value by more than 20%. As reported earlier [23], the sampling frequency and integration time have a significant impact on the performance of the measurement system. The sampling frequency is determined by the frequency characteristics of the electrostatic signals. It is known that the bandwidth of the signal depends on the velocity of particles and the width of the electrode [22]. During fluidization, the velocity of solid particles in the bed is almost lower than 1 m/s. According to the velocity of particles and the width of the electrode (6 mm), the signal bandwidth is estimated to be below 200 Hz. In order to have a higher resolution, the sampling frequency should be set at least ten times the highest frequency of the signal. As a result, the sampling frequency of 2 kHz was used. The integration time depends on the required standard deviation of the correlation velocity and expected response time of the measurement system. In view of the complex flow behavior in the bed, the integration time for each correlation calculation is set to 5 s and 60 correlation results are obtained from each data sample. Average correlation velocity and corresponding standard deviation are calculated from the 60 correlation results.

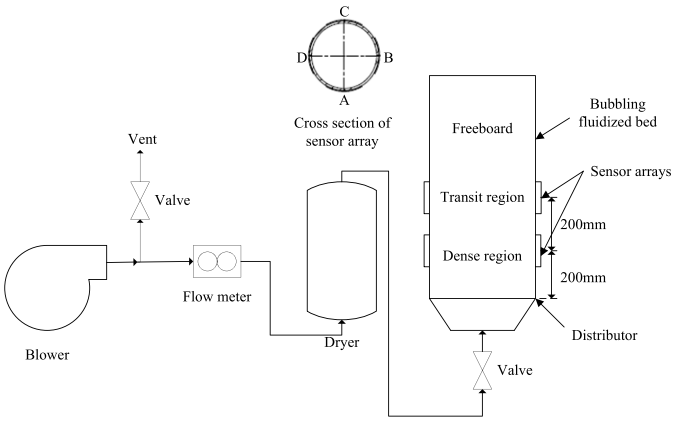

Fig. 4. Layout of the bubbling fluidized test bed.

III. Experimental Setup

Experiments were conducted on a bubbling fluidized test bed. The layout of the test bed is shown in Fig. 4. The fluidized bed is made of transparent Plexiglas with an inner diameter of 150 mm and a height of 1000 mm. A perforated-plate distributor (with a pore diameter of 1.5 mm and an open area ratio of 2.6%) is fitted at the bottom of the bed. During the experiments, polyethylene particles (Geldart A) were fluidized by air from a blower. The relative permittivity of the polyethylene particles is 2.3. The true density of the particles is 918 kg/m^3, which is obtained from the supplier [25]. The particle size ranges from 0.105 to 0.22 mm, as measured using Malvern Mastersizer 2000 [26], whilst the shape of the particles is roughly spherical. The particles were dried before each test run to eliminate humidity effects. The particles were added to the bed, forming a static bed height of 265 mm. The fluidization air flow rate varied from 8 to 16 m^3/h during the experiments, which was measured using a rotameter. The moisture content of the air was reduced by a dryer, which was filled with drying particles. The temperature and relative

humidity of the air before entering the bed were 27 °C and 7.5%, respectively.

When the fluidization air was injected into the bed, the solid particles moved upward due to rising of bubbles and air stream. Besides, small bubbles were coalesced into bigger ones during the upward movements and the big bubbles erupted at the bed surface. In the freeboard, a small number of particles move up and down continuously. The similarity between the signals is, thus, poor leading to invalid solid velocity through correlation. As a result, the lower group of sensors (L group) was fitted at the dense region while the higher group (H group) at the transit region in this paper. In consideration of the inner diameter of the bed (150 mm) and the static bed height (265 mm), L group of the sensor arrays was positioned 200 mm above the air distributor (Fig. 4). Through experimental observations, the area at 400 mm above the air distributor was identified as the transit region of the bed. Solid particles in this region may fall down due to gravity. As a result, the spacing between the L and H groups was set to 200 mm (Fig. 4).

IV. Results and Discussion

A. Time and Frequency Domain Analysis

A typical electrostatic signal sequence in the dense region and its corresponding PSD distribution are plotted in Fig. 5. It can be seen that the randomness of the electrostatic signal is due to the fluctuation of electrostatic charges on the particles and the movement of the particles across the sensing zone of the electrode. The amplitude of the electrostatic signal is determined by the charge distribution and solid velocity in the bed. Fig. 5(b) indicates that the frequency of the signal is low and the highest frequency of the signal is below 200 Hz. In order to investigate the electrostatic charge distribution in the dense region, rms values of the electrostatic signals are calculated, as shown in Fig. 6. The signals are obtained from the three electrodes in set A from the dense region, which are labeled as L-A-1, L-A-2, and L-A-3 from low to high positions. By comparing the rms values of the signals from the three electrodes, it is found that the signal from electrode L-A-3 is higher in magnitude than those from electrodes L-A-1 and L-A-2, which suggests that there are more charges on the particles in the higher position of the dense region. Besides, the signal from the same electrode increases in magnitude with the fluidization air flow rate. The reason for this is that with the increase in fluidization air flow rate, more bubbles are generated in the dense region and the velocity of solid particles increases. Due to the movement of the bubbles and the increase in particle velocity, more interactions between the particles and more frictions between the particles and the wall and between the particles and air occur. As a result, more electrostatic charges are thus generated on the particles.

In order to characterize the power spectra of the electrostatic signals, average fluctuation frequencies of the signals from set A electrodes in the dense region for different fluidization air flow rates are calculated, as shown in Fig. 7. It can be seen from Fig. 7 that the signal from

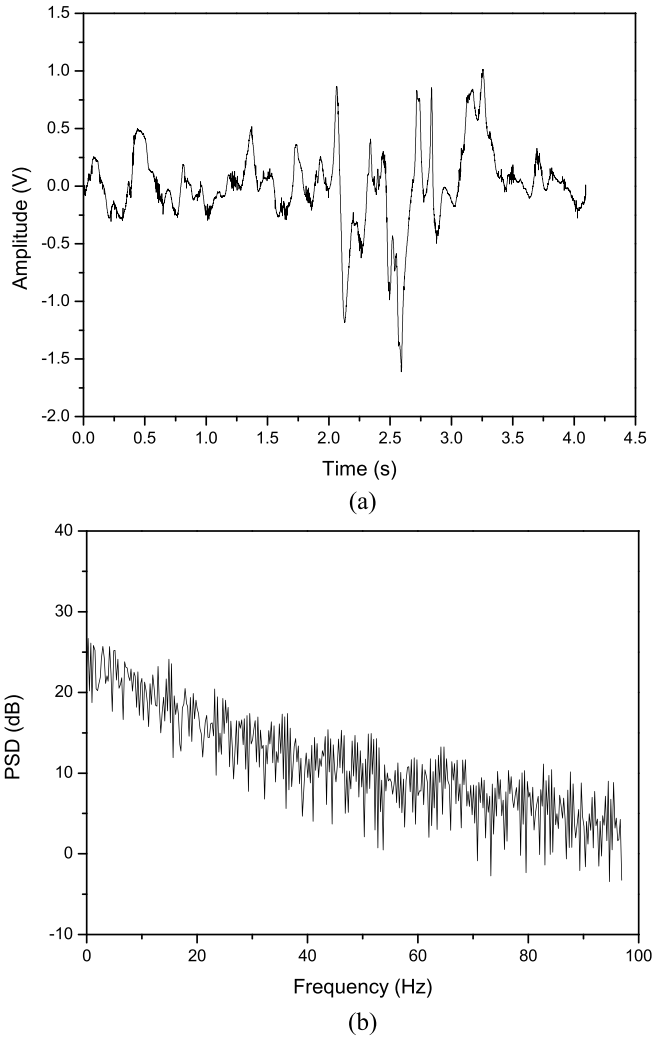

Fig. 5. (a) Typical electrostatic signal from electrode L-A-3 and (b) its PSD distribution for a fluidization air flow rate of 16 m^3/h.

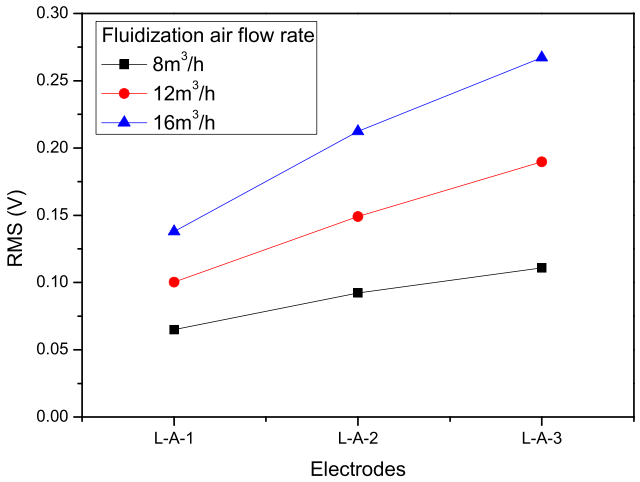

Fig. 6. RMS values of the electrostatic signals from set A electrodes in the dense region for different fluidization air flow rates.

electrode L-A-3 has lower average fluctuation frequency than those from electrodes L-A-1 and L-A-2. There are many small bubbles in the lower position of the dense region. The small bubbles are coalesced into big bubbles, and the number of the bubbles decreases during the upward movement of

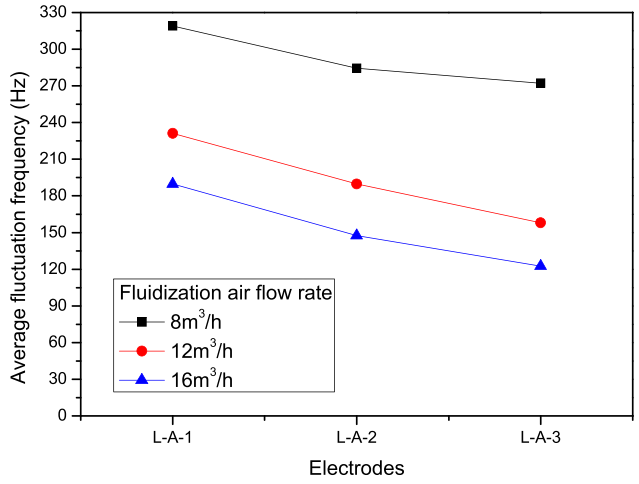

Fig. 7. Average fluctuation frequency of the electrostatic signals from set A electrodes in the dense region of the bed for different fluidization air flow rates.

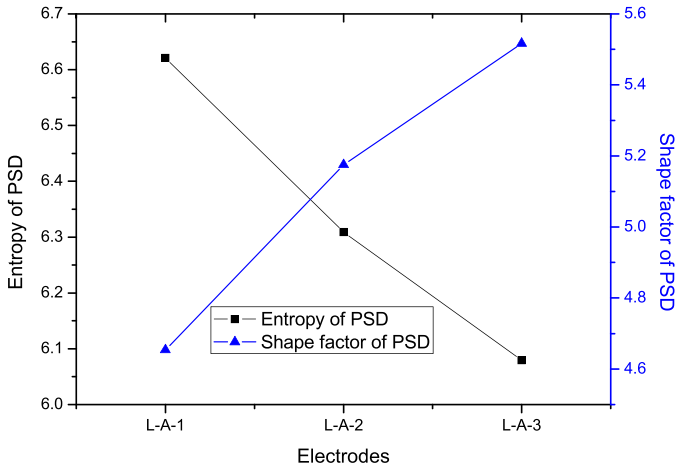

Fig. 8. Entropy and shape factor of PSD of the electrostatic signals from set A electrodes in the dense region for a fluidization air flow rate of 16 m^3/h.

the bubbles. As a result, with more small bubbles, the gas–solid flow in the lower position of the dense region is more turbulent, and hence more higher frequency components in the electrostatic signal from electrode L-A-1. In addition, with the increase in fluidization air flow rate, the average fluctuation frequency of the electrostatic signal from the same electrode decreases. This result is due to the fact that more large particles are fluidized with the aid of higher fluidization air flow rate. However, large particles have lower velocity in the bed. Because the bandwidth of the electrostatic signal is proportional to the solid velocity [22], more large particles result in the increase in lower frequency components in the signal.

To characterize the distribution of PSD, entropy and shape factor of PSD are calculated using (2)–(4). The results of entropy and shape factor of PSD are plotted in Fig. 8. Entropy is a measure of the complexity of PSD. It can be found that PSD of the electrostatic signal from electrode L-A-1 has higher entropy. Thus, the flow dynamics in the lower position of the dense region is more complex, which is consistent with the analysis of the average fluctuation frequency (Fig. 7). Shape factor represents the dispersion degree of PSD.

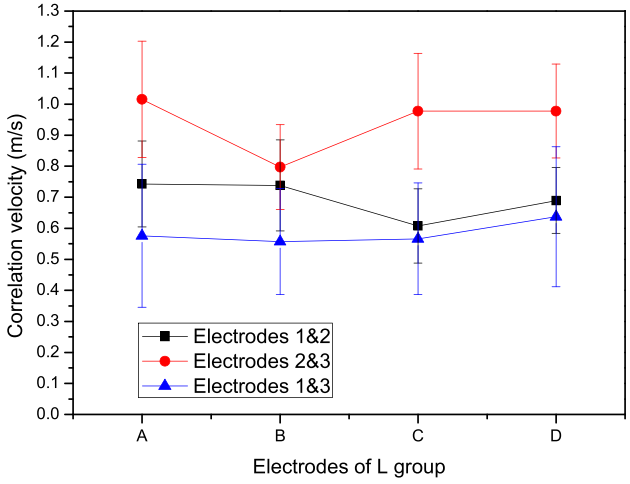

Fig. 9. Average values and corresponding standard deviations of the correlation velocities from the three electrodes in the dense region for a fluidization air flow rate of 16 m^3/h.

It is found that the shape factor of PSD increases with the height of the electrode in the dense region. Therefore, PSD of the electrostatic signal from electrode L-A-3 is more dispersed and has higher bandwidth.

B. Cross Correlation Analysis

Cross correlation analysis of the electrostatic signals from different electrodes in the dense and transit regions for Geldart A particles is performed. The average values of the correlation velocities from the three electrodes in the dense region for fluidization air flow rate of 16 m^3/h are shown in Fig. 9. Standard deviations of the correlation velocities are given as the error bars. The correlation velocities from electrodes 2 and 3 are higher than those from electrodes 1 and 2 due to the fact that with the rising of small bubbles, the particles in the dense region are accelerated. As a result, the velocities from the electrodes in the higher position of the region are greater than those from the lower electrodes. However, because some of the particles in the dense region may fall down near the wall in the higher position of the dense region, the correlation velocity from electrodes 1 and 3 is consistently lower than those from electrodes 1 and 2 and electrodes 2 and 3. Besides, because the longer separation between electrodes 1 and 3 acts as a low-pass filter to eliminate noise, the standard deviation of the correlation velocity from electrodes 1 and 3 is lower than those from electrodes 1 and 2 and electrodes 2 and 3.

Average values and corresponding standard deviations of the correlation coefficients from the three electrodes for Geldart A particles and Geldart D particles are shown in Fig. 10. Correlation coefficient from electrodes 1 and 3 is consistently smaller than those from electrodes 1 and 2 and electrodes 2 and 3 because of the longer separation between the upstream and downstream electrodes and deteriorating flow patterns. In addition, correlation coefficients for Geldart A particles are obviously smaller than those for Geldart D particles [Fig. 10(b)]. Since correlation coefficient is a measure of the similarity between the upstream and downstream signals, it is evident that the flow of Geldart A particles is more turbulent than that of Geldart D particles in the dense region.

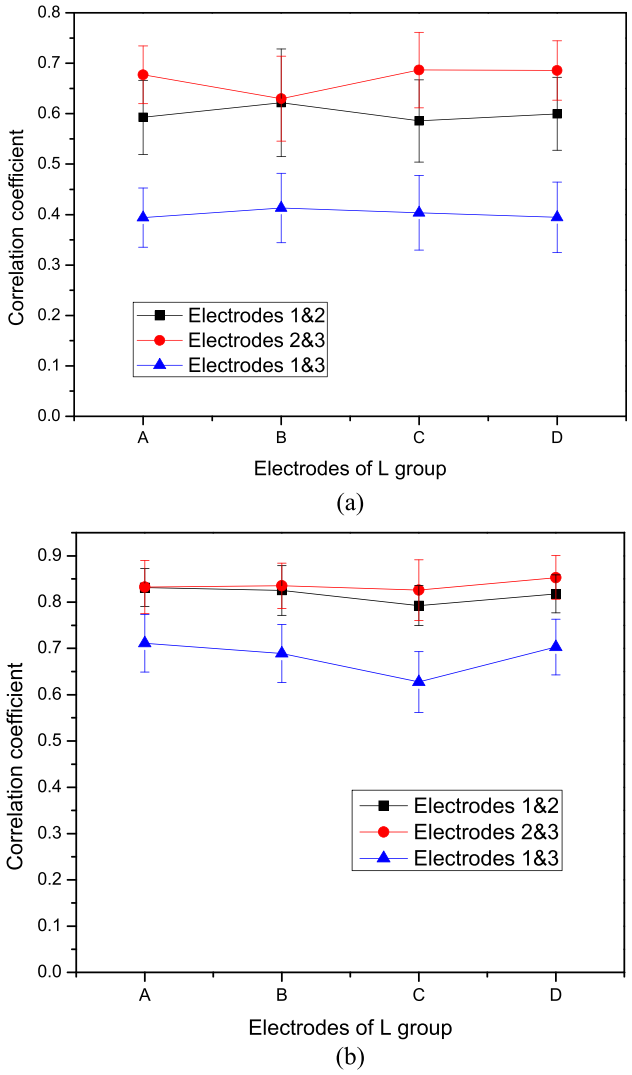

Fig. 10. Average values and corresponding standard deviations of the correlation coefficients from the three electrodes for (a) Geldart A and (b) Geldart D particles.

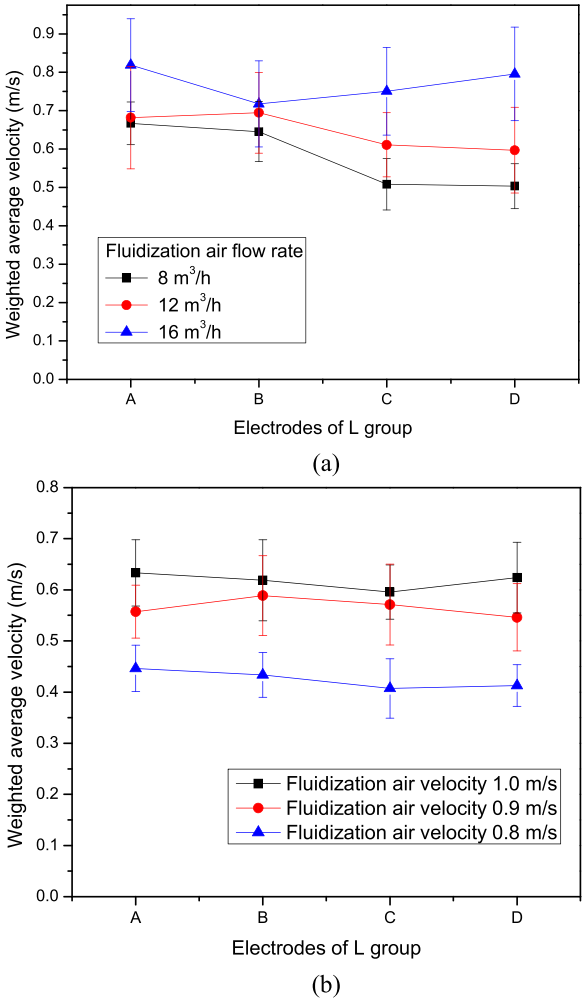

Fig. 11. Weighted average velocities from different sets of electrodes in the dense region for (a) Geldart A and (b) Geldart D particles.

Average values and standard deviations of the weighted average velocities from different sets of electrodes in the dense region for Geldart A particles are plotted in Fig. 11(a). It is clear that the velocity of the bubbles in the bed increases with fluidization air flow rate. Since the particle motion is driven by the bubbles in the bed, the velocity of solid particles increases with the bubble velocity. In addition, the standard deviation of the weighted average velocity is lower than those of the correlation velocities from the three electrodes, suggesting that the three-electrode sensor array provides more reliable results than the conventional two-electrode sensor. In addition, because Geldart A particles are much smaller and lighter than Geldart D particles, the flow dynamics of Geldart A particles in the dense region is more turbulent. As a result, weighted average velocities from different electrodes, which represent the velocity profile of Geldart A particles in the dense region, are not as uniform as that of Geldart D particles [Fig. 11(b)].

A group of electrodes is also installed in the transit region of the bed to investigate the flow dynamics in this region. It is found that the big bubbles erupt at the surface of the bed. Due to eruptions of the bubbles, the particles are splashed upward at first and then drop downward due to gravity. As a result, the flow behavior in this region is more complex. Typical correlation velocities from set A electrodes in the transit region for Geldart A particles are shown in Fig. 12(a). It is revealed that the particles in the lower position of the region mostly move upward, which is shown by the correlation velocities from electrodes 1 and 2. However, in the higher position of the transit region, there are many particles falling downward, which result in the negative correlation velocities from electrodes 2 and 3 and electrodes 1 and 3. In addition, the negative velocity implies that the flow dynamics of Geldart A particles in the transit region is more complex than that of Geldart D particles [Fig. 12(b)].

C. Effects of Liquid Antistatic Agents

LAA will reduce the charge generation rate by the liquid film around the particle, which prohibits the frictions between the particles and the interactions between the particles and the bed wall. Besides, LAA has good conductivity and the charge dissipation rate of fluidized particles will be accelerated after injection of LAA. As a result, the amount of electrostatic

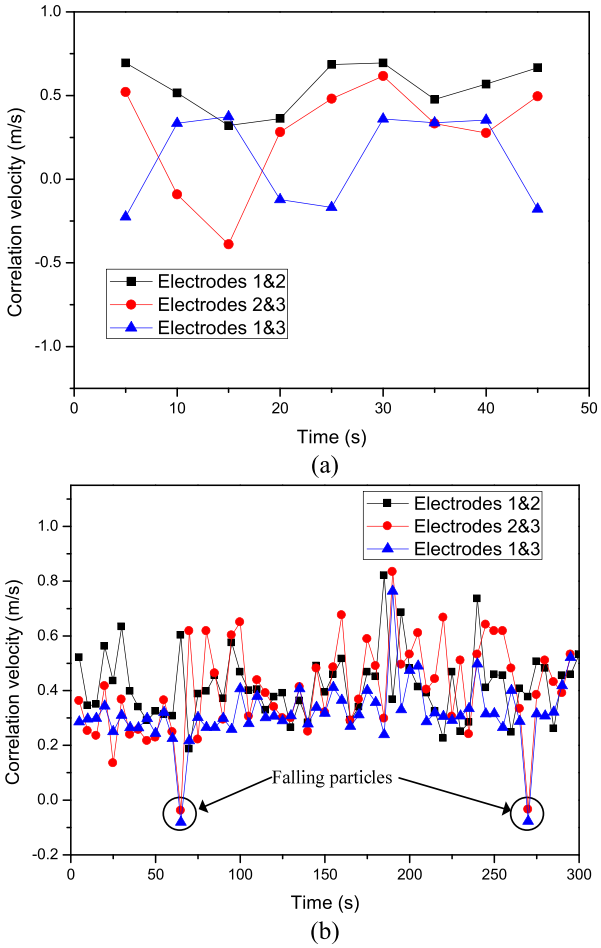

Fig. 12. Typical correlation velocities from set A electrodes in the transit region for (a) Geldart A and (b) Geldart D particles.

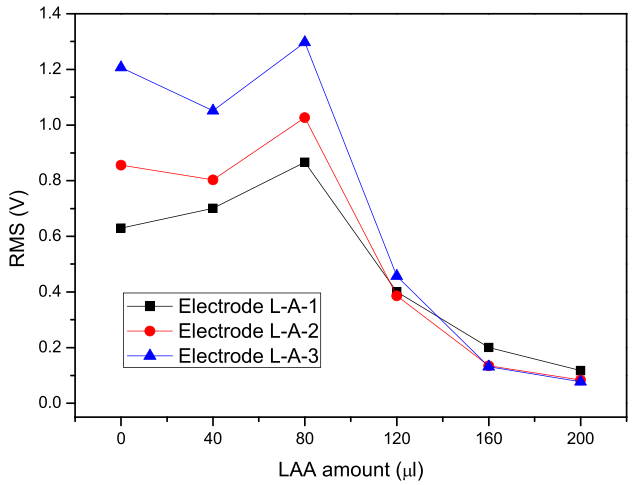

Fig. 13. RMS values of electrostatic signals from set A electrodes in the dense region.

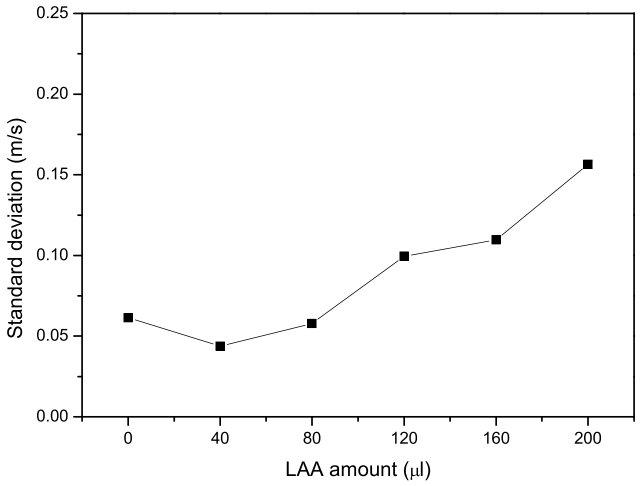

Fig. 14. Standard deviation of the weighted average velocity from set A electrodes in the dense region.

charge on the particles will decrease. During the experiments, a different amount of LAA was injected into the center of the bed close to the distributor (Fig. 4). The injected LAA was dispersed with the aid of a high velocity air jet near the distributor. The electrostatic signals from set A electrodes in the dense region were recorded.

The relationship between the amplitudes of the electrostatic signals and the amount of LAA is investigated. It can be found from Fig. 13 that when the amount of LAA is lower than 80 μL, the rms value of the electrostatic signal from the same electrode does not vary significantly with the amount of LAA. This is likely because the small amount of LAA does not disperse effectively to the whole bed, which will not affect the charge distribution in the bed. When the amount of LAA is beyond 120 μL, the rms value of the electrostatic signal decreases significantly, indicating the reduction of electrostatic charges in the bed. However, when the electrostatic signal is very weak, the correlation velocity becomes less reliable and inaccurate. Fig. 14 shows the standard deviation of the weighted average velocity from set A electrodes in the dense region. It is found that when the amount of LAA is lower than 80 μL, the standard deviation of the weighted averaged velocity is almost independent of the LAA. However, when the amount of LAA is greater than 120 μL, the standard deviation is doubled or tripled compared to that without LAA. This suggests that the addition to LAA affects the validity of the measured correlation velocity.

V. Conclusion

Multiple electrostatic sensor arrays have been used to investigate the flow dynamics of solid particles in a bubbling fluidized bed. RMS amplitudes of the sensor signals have revealed that there are more electrostatic charges generated in the higher part of the dense region. In addition, the electrostatic charge increases with the fluidization air flow rate. It is found through frequency analysis that the flow dynamics in the lower part of the dense region is more turbulent. The correlation velocities and weighted average velocity of Geldart A particles in the dense and transit regions are determined through cross correlation computation and data fusion. Due to the smaller size and lower density, the velocity profile of Geldart A particles in the dense region is not as uniform as that of Geldart D particles and the flow behavior of Geldart A particles in the transit region is more complex

than that of Geldart D particles. The effect of LAA on the performance of electrostatic sensor arrays has been investigated. When the amount of LAA is greater than 120 μL, the standard deviation of the weighted averaged velocity significantly increases with LAA.

The experimental results presented in this paper have suggested that the flow characteristics in the dense and transit regions can be measured using electrostatic sensor arrays. Both time and frequency domain methods are found effective in quantifying the flow behaviors of the particles and charge distribution. Furthermore, it is estimated that for the fluidized test bed, the amount of LAA between 80 and 120 μL may be a good choice to not only control the electrification of solid particles in the bed but also ensure the performance of the electrostatic sensor arrays. As the solids distribution is an important parameter in fluidized bed operation, measurement of solids concentration distribution will be investigated in the future.

REFERENCES

[1] J. R. van Ommen and R. F. Mudde, "Measuring the gas–solids distribution in fluidized beds—A review," *Int. J. Chem. Reactor Eng.*, vol. 6, no. 1, pp. 1–29, 2008.

[2] J. Wang, Y. Cao, X. Jiang, and Y. Yang, "Agglomeration detection by acoustic emission (AE) sensors in fluidized beds," *Ind. Eng. Chem. Res.*, vol. 48, no. 7, pp. 3466–3473, 2009.

[3] J. Wang, C. Ren, Y. Yang, and L. Hou, "Characterization of particle fluidization pattern in a gas solid fluidized bed based on acoustic emission (AE) measurement," *Ind. Eng. Chem. Res.*, vol. 48, no. 18, pp. 8508–8514, 2009.

[4] J. Wang, C. Ren, and Y. Yang, "Characterization of flow regime transition and particle motion using acoustic emission measurement in a gas–solid fluidized bed," *AIChE J.*, vol. 56, no. 5, pp. 1173–1183, 2010.

[5] G. Hendrickson, "Electrostatics and gas phase fluidized bed polymerization reactor wall sheeting," *Chem. Eng. Sci.*, vol. 61, no. 4, pp. 1041–1064, 2006.

[6] J. Ma and Y. Yan, "Design and evaluation of electrostatic sensors for the measurement of velocity of pneumatically conveyed solids," *Flow Meas. Instrum.*, vol. 11, no. 3, pp. 195–204, 2000.

[7] Y. Yan, L. Xu, and P. Lee, "Mass flow measurement of fine particles in a pneumatic suspension using electrostatic sensing and neural network techniques," *IEEE Trans. Instrum. Meas.*, vol. 55, no. 6, pp. 2330–2334, Dec. 2006.

[8] J. Shao, J. Krabicka, and Y. Yan, "Velocity measurement of pneumatically conveyed particles using intrusive electrostatic sensors," *IEEE Trans. Instrum. Meas.*, vol. 59, no. 5, pp. 1477–1484, May 2010.

[9] W. Zhang, C. Wang, and H. Wang, "Hilbert–Huang transform-based electrostatic signal analysis of ring-shape electrodes with different widths," *IEEE Trans. Instrum. Meas.*, vol. 61, no. 5, pp. 1209–1217, May 2012.

[10] X. Qian and Y. Yan, "Flow measurement of biomass and blended biomass fuels in pneumatic conveying pipelines using electrostatic sensor-arrays," *IEEE Trans. Instrum. Meas.*, vol. 61, no. 5, pp. 1343–1352, May 2012.

[11] X. Qian, Y. Yan, J. Shao, L. Wang, H. Zhou, and C. Wang, "Quantitative characterization of pulverized coal and biomass–coal blends in pneumatic conveying pipelines using electrostatic sensor arrays and data fusion techniques," *Meas. Sci. Technol.*, vol. 23, no. 8, p. 085307, 2012.

[12] X. Qian, X. Huang, Y. Hu, and Y. Yan, "Pulverized coal flow metering on a full-scale power plant using electrostatic sensor arrays," *Flow Meas. Instrum.*, vol. 40, pp. 185–191, Dec. 2014.

[13] F. Portoghese, F. Berruti, and C. Briens, "Continuous on-line measurement of solid moisture content during fluidized bed drying using triboelectric probes," *Powder Technol.*, vol. 181, no. 2, pp. 169–177, 2008.

[14] W. Zhang, Y. Cheng, C. Wang, W. Yang, and C.-H. Wang, "Investigation on hydrodynamics of triple-bed combined circulating fluidized bed using electrostatic sensor and electrical capacitance tomography," *Ind. Eng. Chem. Res.*, vol. 52, no. 32, pp. 11198–11207, 2013.

[15] C. He, X. T. Bi, and J. R. Grace, "Simultaneous measurements of particle charge density and bubble properties in gas-solid fluidized beds by dual-tip electrostatic probes," *Chem. Eng. Sci.*, vol. 123, pp. 11–21, Feb. 2015.

[16] C. He, X. T. Bi, and J. R. Grace, "A novel dual-material probe for *in situ* measurement of particle charge densities in gas–solid fluidized beds," *Particuology*, vol. 21, pp. 20–31, Aug. 2015.

[17] D. Geldart, "Types of gas fluidization," *Powder Technol.*, vol. 7, no. 5, pp. 285–292, 1973.

[18] W. Zhang, Y. Yan, Y. Yang, and J. Wang, "Measurement of flow parameters in a bubbling fluidized bed using electrostatic sensor arrays," in *Proc. IEEE Int. Instrum. Meas. Technol. Conf.*, Pisa, Italy, May 2015, pp. 1573–1577.

[19] A.-H. Park, H. Bi, and J. R. Grace, "Reduction of electrostatic charges in gas–solid fluidized beds," *Chem. Eng. Sci.*, vol. 57, no. 1, pp. 153–162, 2002.

[20] J. Wang, Y. Xu, W. Li, Y. Yang, and F. Wang, "Electrostatic potentials in gas–solid fluidized beds influenced by the injection of charge inducing agents," *J. Electrostatics*, vol. 67, no. 5, pp. 815–826, 2009.

[21] K. Dong, Q. Zhang, Z. Huang, Z. Liao, J. Wang, and Y. Yang, "Experimental investigation of electrostatic effect on bubble behaviors in gas–solid fluidized bed," *AIChE J.*, vol. 61, no. 4, pp. 1160–1171, 2015.

[22] Y. Yan, B. Byrne, S. Woodhead, and J. Coulthard, "Velocity measurement of pneumatically conveyed solids using electrodynamic sensors," *Meas. Sci. Technol.*, vol. 6, no. 5, pp. 515–537, 1995.

[23] W. Zhang, C. Wang, and Y. Wang, "Parameter selection in cross-correlation-based velocimetry using circular electrostatic sensors," *IEEE Trans. Instrum. Meas.*, vol. 59, no. 5, pp. 1268–1275, May 2010.

[24] J. J. Nieuwland, R. Meijer, J. A. M. Kuipers, and W. P. M. van Swaaij, "Measurements of solids concentration and axial solids velocity in gas-solid two-phase flows," *Powder Technol.*, vol. 87, no. 2, pp. 127–139, 1996.

[25] E. H. Higham and W. Boyes, "Measurement of density," in *Instrumentation Reference Book*, 3rd ed. Oxford, U.K.: Butterworth, 2003, pp. 114–122.

[26] *Mastersizer 2000 User Manual*, Malvern Instrum., Malvern, U.K., 1999.

Wenbiao Zhang (M'15) received the B.Sc. degree in automation, and the M.Eng. and Ph.D. degrees in measurement technology and automatic devices from Tianjin University, Tianjin, China, in 2008, 2010, and 2014, respectively.

He is currently a Lecturer with the School of Control and Computer Engineering, North China Electric Power University, Beijing, China. His current research interests include measurement of flow parameters in pneumatic conveying process and fluidized bed.

Yong Yan (M'04–SM'04–F'11) received the B.Eng. and M.Sc. degrees in instrumentation and control engineering from Tsinghua University, Beijing, China, in 1985 and 1988, respectively, and the Ph.D. degree in flow measurement and instrumentation from the University of Teesside, Middlesbrough, U.K., in 1992.

He is currently a Professor of Electronic Instrumentation and the Director of Research with the School of Engineering and Digital Arts, University of Kent, Canterbury, U.K. He has published in excess of 300 research papers in journals and conference proceedings with an h-index of 33.

Yongrong Yang received the B.Sc., M.Sc., and Ph.D. degrees from Zhejiang University, Hangzhou, China, in 1984, 1986, and 1989, respectively, all in chemical engineering.

He is currently a Professor with the School of Chemical and Biological Engineering, Zhejiang University. His current research interests include multiphase flow reaction engineering, polymerization engineering, and process system engineering.

Jingdai Wang received the B.Sc., M.Sc., and Ph.D. degrees from Zhejiang University, Hangzhou, China, in 1996, 1999, and 2002, respectively, all in chemical engineering.

He is currently a Professor with the School of Chemical and Biological Engineering, Zhejiang University. His current research interests include multiphase flow reaction engineering, polymerization engineering, and process system engineering.